Electrically driven hybrid Si/III-V Fabry-Pérot lasers based on adiabatic mode transformers

B. Ben Bakir[*], A. Descos, N. Olivier, D. Bordel, P. Grosse, E. Augendre, L. Fulbert, and J. M. Fedeli

CEA-LETI, Minatec, 17 rue des Martyrs, F-38054 Grenoble cedex 9, France
[*]*badhise.ben-bakir@cea.fr*

Abstract: We report the first demonstration of an electrically driven hybrid silicon/III–V laser based on adiabatic mode transformers. The hybrid structure is formed by two vertically superimposed waveguides separated by a 100-nm-thick SiO_2 layer. The top waveguide, fabricated in an InP/InGaAsP-based heterostructure, serves to provide optical gain. The bottom Si-waveguides system, which supports all optical functions, is constituted by two tapered rib-waveguides (mode transformers), two distributed Bragg reflectors (DBRs) and a surface-grating coupler. The supermodes of this hybrid structure are controlled by an appropriate design of the tapers located at the edges of the gain region. In the middle part of the device almost all the field resides in the III–V waveguide so that the optical mode experiences maximal gain, while in regions near the III-V facets, mode transformers ensure an efficient transfer of the power flow towards Si-waveguides. The investigated device operates under quasi-continuous wave regime. The room temperature threshold current is 100 mA, the side-mode suppression ratio is as high as 20 dB, and the fiber-coupled output power is ~7 mW.

©2011 Optical Society of America

OCIS codes: (140.5960) Semiconductor lasers; (250.5300) Photonic integrated circuits.

References and links

1. G.T. Reed, "The optical age of silicon," Nature, **427**, 595-596 (2004).
2. B. Corcoran, C. Monat, M. Pelusi, C. Grillet, T. P. White, L. O'Faolain, T. F. Krauss, B. J. Eggleton, and D. J. Moss, "Optical signal processing on a silicon chip at 640Gb/s using slow-light," Opt. Express, **18**, 7770-7781 (2010).
3. Silicon photonics II, edited by D. Lockwood and L. Pavesi, Topics in Applied Physics, Springer Verlag (2010).
4. B. Ben Bakir, A. Vazquez de Gyves, R. Orobtchouk, P. Lyan, C. Porzier, A. Roman, and J-M. Fedeli, "Low loss (<1dB) and Polarization-Insensitive Edge Fiber Couplers fabricated on 200 mm Silicon-on-Insulator wafers," IEEE Phot. Tech. Letters, **22**, 739-741 (2010).
5. K. K. Lee, D. R. Lim, D. Pan, C. Hoepfner, W-Y. Oh, K. Wada, L.C. Kimerling, K.P. Yap, M.T. Doan, "Mode transformer for miniaturized optical circuits," Opt. Lett., **30**, 498-500 (2005).
6. W. Bogaerts, S. Selvaraja, P. Dumon, J. Brouckaert, K. De Vos, D. Van Thourhout, R. Baets, "Silicon-on-Insulator Spectral Filters Fabricated with CMOS Technology", (invited) J. Sel. Top. Quantum Electron., **16**, 33-44 (2010).
7. D. Marris-Morini, L. Vivien, J-M. Fédéli, E. Cassan, Ph. Lyan, S. Laval, "Low loss and high speed silicon optical modulator based on a lateral carrier depletion structure," Opt. Express, **16**, 334-339 (2008).
8. L. Vivien, M. Rouvière, J-M Fédéli, D. Marris-Morini, J.F. Damlencourt, J. Mangeney, P. Crozat, L. El Melhaoui, E. Cassan, X. Le Roux, D. Pascal, and S. Laval, "High speed and high responsivity germanium photodetector integrated in a Silicon-On-Insulator microwaveguide," Opt. Express, **15**, 9843-9848 (2007).
9. J.M. Fedeli *et al.*, "Development of Silicon Photonics Devices Using Microelectronic Tools for the Integration on Top of a CMOS Wafer," Advances in Optical Technologies, **2008**, 412518 (2008).
10. H. Kromer, T.-Y. Liu, and P. M. Petroff, "GaAs on Si and related systems: Problems and prospects," J. Cryst. Growth, **95**, 96-102 (1989).
11. O. Boyraz, and B. Jalali, "Demonstration of a silicon Raman laser," Opt. Express, **12**, 5269 (2004).
12. H. Rong, "A continuous-wave Raman silicon laser," Nature, **433**, 725-728 (2005).

13. B. Gelloz, A. Kojima, and N. Koshida, “Highly efficient and stable luminescence of nanocrystalline porous silicon treated by high-pressure water vapor annealing,” Appl. Phys. Lett., **87**, 031107 (2005).
14. L. Pavesi, L. Dal Negro, C. Mazzoleni, G. Franzò, and F. Priolo, “Optical gain in silicon nanocrystals,” Nature, **408**, 440–444 (2000).
15. K. Solehmainen, M. Kapulainen, P. Heimala, and K. Polamo, “Erbium doped waveguides fabricated with atomic layer deposition method,” IEEE Phot. Tech. Letters, **16**, 194–196 (2004).
16. J. Liu, X. Sun, R. C. Aguilera, L. C. Kimerling, and J. Michel, “Ge-on-Si laser operating at room temperature,” Opt. Lett., **35**, 679-681 (2010).
17. K. Kato, and Y. Tohmori, “PLC hybrid integration technology and its application to photonic components,” IEEE J. Sel. Tops. Quantum Electron, **6**, 4-13 (2000).
18. J. Sasaki, M. Itoh, .T. Tamanuki, H. Hatakeyama, S. Kitamura, T. Shimoda, T. Kato, “Multiple-chip precise self-aligned assembly for hybrid integrated optical modules using Au–Sn solder bumps,” IEEE Transactions on Advanced Packaging, **24**, 569-575 (2001).
19. G. Roelkens, L. Liu, D. Liang, R. Jones, A. W. Fang, B. R. Koch, and J.E. Bowers, “III-V/silicon photonics for on-chip and intra-chip optical interconnects,” Laser & Photon. Rev., **4**, 751-779 (2010).
20. A. W. Fang, H. Park, O. Cohen, R. Jones, M. J. Paniccia, and J. E. Bowers, “Electrically pumped hybrid AlGaInAs-silicon evanescent laser,” Opt. Express, **14**, 9203 -9210 (2006).
21. X. Sun, A. Zadok, M. J. Shearn, K.A. Diest, A. Ghaffari, H.A. Atwater, A. Scherer, and A. Yariv, “Electrically pumped hybrid evanescent Si/InGaAsP lasers,” Opt. Lett., **34**, 1345-1347 (2009).
22. A. W. Fang, R. Jones, H. Park, O. Cohen, O. Raday, M. J. Paniccia, and J. E. Bowers, “Integrated AlGaInAs-silicon evanescent race track laser and photodetector,” Opt. Express, **15**, 2315-2322 (2007).
23. A. W. Fang, E. Lively, Y.-H. Kuo, D. Liang, and J. E.Bowers, “A distributed feedback silicon evanescent laser,” Opt. Express, **16**, 4413-4419 (2008).
24. A. Yariv and X. K. Sun, “Supermode Si/ III–V hybrid lasers, optical amplifiers and modulators: a proposal and analysis,” Opt. Express, **15**, 9147–9151 (2007).
25. X. Sun and A. Yariv, “Engineering supermode silicon/III–V hybrid waveguides for laser oscillation,” J. Opt. Soc. Am. B, **25**, 923-926 (2008).
26. X. Sun, H.-C. Liu, and A. Yariv, “Adiabaticity criterion and the shortest adiabatic mode transformer in a coupled-waveguide system,” Opt. Lett., **34**, 280-282 (2009).
27. A. Karim, *et al.* “Super lattice barrier 1528-nm vertical-cavity laser with 85°C continuous-wave operation,” IEEE Photon. Technol. Lett., **12**, 1438-1440 (2000).
28. M. Kostrzewa, L. Di Cioccio, M. Zussy, J.C Roussin, J.M Fedeli, N. Kernevez, P. Regreny, C. Lagahe-Blanchard, B. Aspar “InP dies transferred onto silicon substrate for optical interconnects application”, Sensors and Actuators A, **125**, 411-414 (2006).
29. A. Katz, B.E. Weir, and W.C. Dautremont-Smith, “Au/Pt/Ti contacts to p-In0.53Ga0.47As and n-InP layers formed by a single metallization step and rapid thermal processing,” J. Appl. Phys., **68**, 1123-1128 (1990).

---

1. Introduction

Silicon photonics has generated an outstanding interest for optical telecommunications [1] and signal processing [2], and for inter- and intra-chip interconnects in microelectronic systems [3]. The development of basic building blocks such as waveguides, I/O couplers [4, 5], wave-division multiplexers [6], modulators [7] and photodetectors [8] has reached such a performance level that the integration challenge of silicon photonics with microelectronics is now considered as an emerging active research area. The underlying technical interest of silicon photonics is the enhancement of performances by closely linking the electronic functions with the integrated optics ones on the same chip. Furthermore, these hybrid electronic-photonic circuits can also benefit from the mass production using lithography and etching processes of a standard CMOS line, thus reducing the fabrication costs [9].

Silicon-based compounds are commonly used in commercial optical waveguide devices for applications such as passive optical interconnects and biomedical sensors. However, the integration of lasers together with Si integrated photonics-electronic circuits has proved to be much more challenging. The complexity lies in the fact that silicon is a poor light-emitting material due to its indirect energy bandgap. In addition, the direct growth of standard III-V materials on Si substrates is still a major obstacle because of the mismatch in lattice constants and in thermal expansion coefficients [10]. Although light emission from silicon is not

straightforward, the development of an efficient electrically pumped laser is essential to make silicon the material of choice for monolithic optoelectronic integration.

Various solutions have been investigated to avoid this intrinsic limitation of silicon by using the Raman amplification effect [11, 12] or materials such as nano-porous silicon [13], silicon nano-crystals [14], rare-earth doped silica glasses [15] and strained germanium-on-silicon [16]. While these demonstrations represent a significant progress, the critical missing element is electrical pumping, since an external light source is necessary to pump the devices and achieve laser emission. A different way consists in coupling laser beams emerging from III-V heterostructures to silicon waveguides. This so-called hybrid integration can be done using different techniques like flip-chip bonding [17] or self assembly [18]. All of them present the disadvantage of requiring submicron precision alignment to enable efficient coupling between lasers and silicon waveguides. Even if the cost of a silicon photonic circuit is generally low, aligning precisely a laser chip to a planar photonic circuit is quite expensive, time consuming and not adapted for high-volume fabrication.

A particularly promising approach is based on molecular bonding of III-V material on top of a patterned Si-on-Insulator (SOI) substrate [9, 28]. This can be performed at the die or wafer level, depending on the application needs. Then, hybrid Si/III-V lasers are realized following a collective fabrication procedure, enabling complex photonic integrated systems onto the silicon platform [19]. Using this technology, Fabry–Pérot [20, 21], racetrack [22], and distributed feedback lasers [23] were demonstrated. Most often, the bonded structure is designed to support a common optical mode, whose electromagnetic field is distributed between the III-V structure and the underlying Si waveguide. In fact, the major part of the field is located in the silicon waveguide and only a few percent, i.e. the tail of the optical mode, overlaps with the multiple quantum wells of the III-V active region. The laser mode is then mainly concentrated in the passive silicon waveguide to the detriment of the modal gain. Another difficulty of this approach is the tight control of the low-index bonding layer, whose thickness must be kept as thin as possible, typically lower than 10 nm. This technological constraint is a limiting factor for the design and the fabrication process. These innovative evanescently-coupled laser structures have obviously several attractive features; however, they use III-V material inefficiently since there is a trade-off to find between the modal gain and the output coupling efficiency.

In this paper, we report on the first experimental demonstration of an electrically driven hybrid Si/III-V laser which is based on the supermode control of a two coupled waveguides system. This approach has been recently discussed in theoretical works [24-26]. The proposed architecture overcomes this tricky compromise between modal gain and coupling efficiency, inherent in the Si evanescent lasers previously reported. The novelty is that the optical supermode is fashioned along the cavity length in order to obtain a strong overlap with the gain region (rather than the evanescent tail) while maintaining a high coupling efficiency with the bottom silicon waveguide. This results in a larger gain available for amplification and, theoretically, an increased efficiency.

The hybrid structure illustrated in Fig. 1 is formed by two vertically superimposed waveguides separated by a 100-nm-thick SiO_2 layer. The top waveguide, fabricated in an InP/InGaAsP-based heterostructure, serves to provide optical gain. The bottom Si-waveguides system, which supports all optical functions, is constituted by two tapered rib-waveguides (mode transformers), two distributed Bragg reflectors (DBRs) and a surface-grating coupler. The optical cavity is defined by the two DBRs spaced 1040 µm apart. Modal reflectivities higher than 90% and 50% were calculated for the back and front mirrors, respectively. The 950-µm-long III-V waveguide (amplifying medium) is placed inside the cavity. The mode transformers, positioned below the edges of the active waveguide, provide an adiabatic transition by varying the width of the Si rib-waveguide. In the middle part of the device, almost all the field resides in the III–V waveguide so that the optical mode experiences maximal gain (Fig 2a), while in regions near the III-V facets, mode transformers ensure an

efficient coupling between the two levels. Then, the output grating coupler ensures the transfer of the power flow towards the multimode fiber.

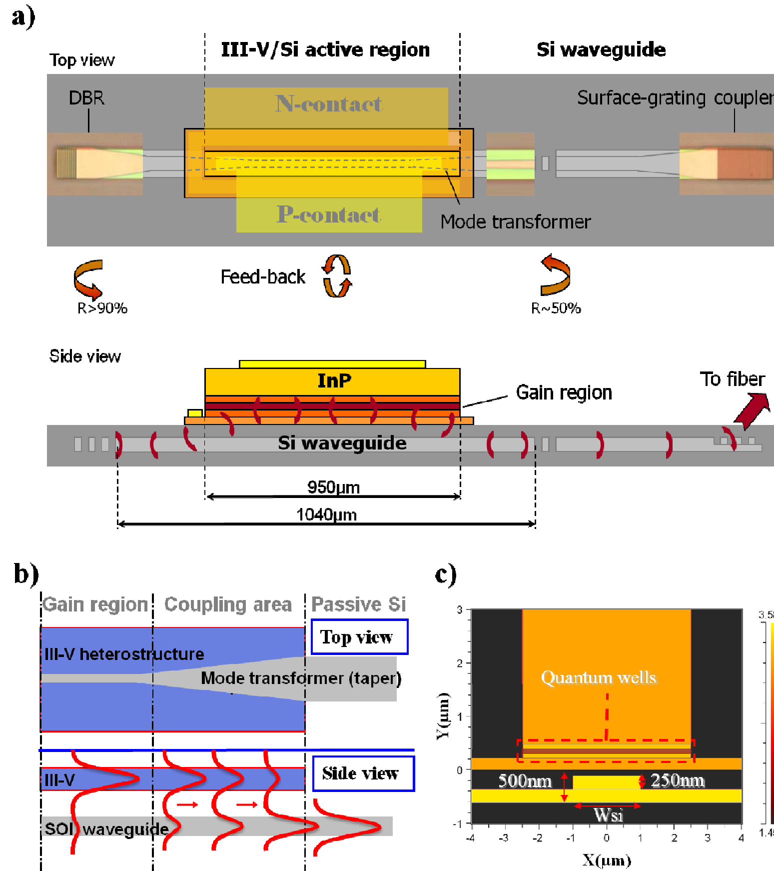

Fig. 1. a) A schematic representation of the hybrid Si/III-V laser with superimposed optical microscope images of each building-block constituting the underlying Si photonic circuit. b) Top and side views of a taper (mode transformer) showing the transfer of the supermode from the upper active waveguide to the lower silicon waveguide. c) A cross-section of the refractive index profile of the structure. The top InGaAsP/InP waveguide width is 5 µm. The Si waveguide is defined by a rib height *H* and a slab height *h* of 500 nm and 250 nm, respectively.

Figure 2(b) presents the electric field patterns (quasi-TE case) for various cross-sections of the mode transformer. Simulations were performed at 1.55 µm by using the beam propagation method. The tapered waveguide is defined by a rib height *H* and a slab height *h*, of 500 nm and 250 nm, respectively. The width of the rib *W* is widened adiabatically from 0.7 µm to 1.1 µm: such variation of the rib width is carried out on a length of 120µm. Both the shape of the mode transformers and, in particular, the thickness of the oxide separation layer are optimized to be robust enough with respect to the variations induced by the fabrication processes. For specific configurations, coupling efficiencies higher than 97% were calculated. In addition, if we take into accounts fabrication process tolerances, the lower limit is found to be ~90%.

A complete analysis of the coupling scheme as well as detailed descriptions of each building-block constituting the laser structure (DBR, grating coupler) will be presented in a forthcoming paper.

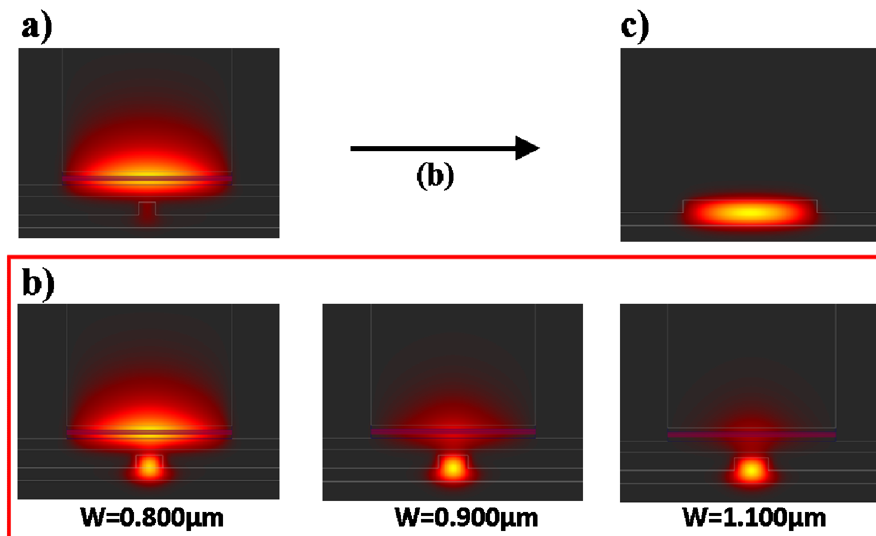

Fig. 2. Evolution of the lasing supermode inside the hybrid Fabry-Pérot cavity. a) Supermode profile in the middle part of the structure. b) Mode transformer: transfer of the supermode power by adiabatically widening the width of the silicon waveguide. c) Fundamental mode of the Si waveguide.

2. Device structure, fabrication and integration

The laser structures are fabricated using mainly CMOS technology. The SOI substrate (200 mm wafer manufactured by SOITEC) used in this work is composed of a mono-crystalline silicon layer with a typical thickness of 500 nm on top of a 2-µm-thick buried oxide layer on a silicon substrate. Figure 1 shows schematic representations of passive devices constituting the bottom silicon level of the laser structure. Three successive steps of lithography were carried out to form various etching depths in the silicon layer. For each sequence, after a silica hard mask deposition, the structure pattern is defined by means of a 193-nm deep-UV lithography followed by hard mask etching and photoresist stripping. The pattern is transferred to the silicon layer by means of a HBr dry etching process. The entire waveguiding structure is then covered by a 500-nm-thick cap layer of silica deposited by plasma-enhanced chemical vapor deposition (PECVD). A chemical-mechanical polishing (CMP) step planarizes the pattern, leaving only an average of 100-nm of silica capping layer. The additional role of CMP is to adjust the thickness of the silicon dioxide cladding layer in order to satisfy the optical coupling conditions.

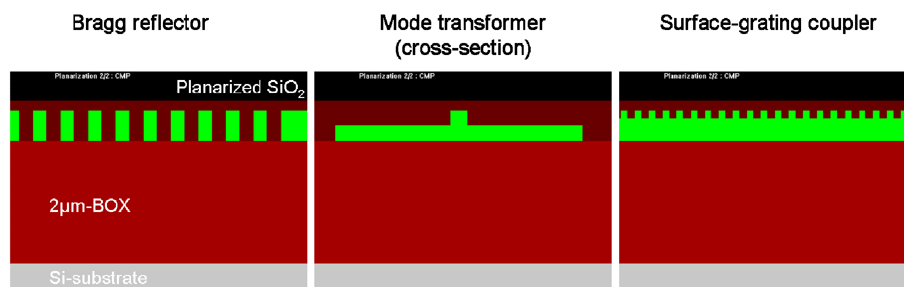

Fig. 3. Schematic representations of passive devices constituting the bottom silicon level of the laser structure. Bragg reflector: the period (Λ) is 650 nm, the etch depth (e) and the duty cycle (dc) are 500 nm and 50%, respectively. Mode transformer: the rib height H and the slab height h are 500 nm and 250 nm, respectively. The width of the rib W varies from 0.7 to 1.1 µm. Surface-grating coupler: Λ=590 nm, e=125nm and dc=50%.

Meanwhile, the III-V epitaxial structure is grown on a 550-µm-thick InP substrate. The details of the InP and InGaAsP layers are presented in Table 1. This III-V heterostructure is similar to the one presented in reference [21]. The waveguiding active region is bounded by separate confinement layers and *n/p*-doped layers. The superlattice is used to prevent the propagation of defects from the bonded layer into the quantum wells region [27].

Table 1. III-V epitaxial growth layer structure.

Layer	Material	Bandgap (eV)	Doping (cm^{-3})	Thickness (nm)
p-contact layer	$In_{0,53}Ga_{0,47}As$	0.77	1.5×10^{19}	300
p-cladding layers	InGaAsP	1.13	2.0×10^{18}	30
	InP	1.34	$1.5 \times 10^{18} \rightarrow 5.0 \times 10^{17}$	2300
Separate confinement layer	InGaAsP	1.06	Undoped	80
Quantum wells	InGaAsP (x6)	0.8	Undoped	8
Barriers	InGaAsP (x5)	1.06	Undoped	10
Separate confinement layer	InGaAsP	1.06	Undoped	80
n-contact layer	InP	1.34	2.0×10^{18}	100
	InGaAsP	1.08	5.0×10^{18}	10
	InP	1.34	2.0×10^{18}	70
Superlattice	InGaAsP (x2)	1.13	1.0×10^{18}	7.5
	InP (x2)	1.34	1.0×10^{18}	7.5
Bonding interface	InP	1.34	Undoped	10

Then, a 10-nm-thick oxide layer was grown on top of the III-V heterostructure prior to dicing the wafer into individual dies. The III-V die size is 7 mm x 7 mm.

The bonding procedure begins with both ozone exposure and soft chemical-mechanical cleaning of III-V and SOI surfaces. The surfaces are activated through a second exposure to oxygen plasma and placed in physical contact at room temperature. The bonding itself occurs spontaneously at room temperature, however, hybrid structures are annealed at 250 °C for 3 hours to reinforce the bonding energy. Dies are then prepositioned to the required places on the SOI wafer, i.e. only where it is needed. Using this technique, where the III-V dies are bonded unprocessed, no precise positioning is required during the bonding step since the accurate alignment between the silicon passive circuits and the III-V active waveguides is given by the lithography resolution, which is typically +/- 50nm for a standard 193-nm deep-UV stepper. A detailed description of the die-to-wafer bonding process can be found in our previous work [28].

Following the bonding, InP substrates are removed by HCl/H_2O wet etching. The 5-µm-wide active waveguides, centered above the Si waveguides, are formed in the InP and InGaAsP layers through deep UV lithography and subsequent etching down to the *n*-InP contact layer (see Table 1). The etching steps are: CH_4/H_2 based plasma reactive ion etching (RIE) through the *p*-InP layers and $H_2SO_4/H_2O_2/H_2O$ (1:1:10, t=50 s) selective wet etching of the quantum well layers to the *n*-type layers. The mesa is then finally defined by photolithography and dry etching of the remaining thin *n*-doped layers.

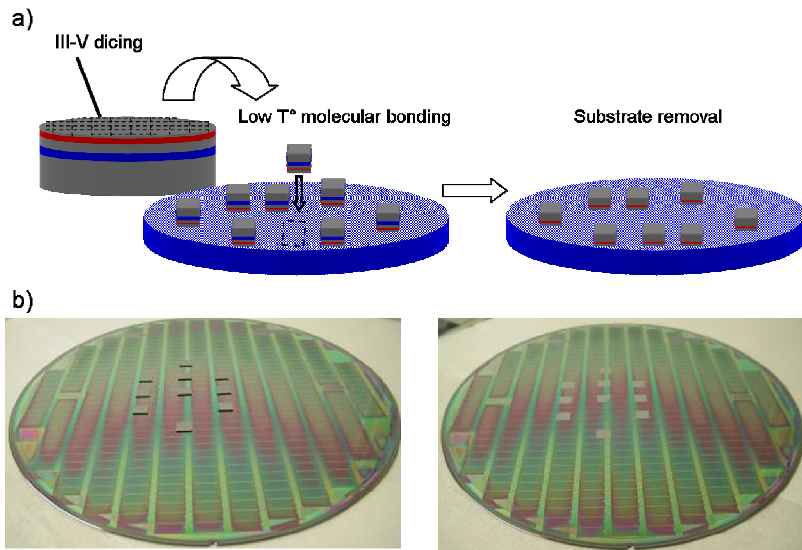

Fig. 4. Schematics of the die-to-wafer bonding process. b) Photos of dies bonded on a patterned 200 mm SOI wafer, before and after substrate removal.

Ni/AuGe/Ni/Au alloy *n*-contacts are deposited onto the exposed *n*-type InP layer, 7 µm away from the center of the silicon waveguide. 3-µm-wide Ti/Pt/Au *p*-contacts are then deposited on the center of the III-V waveguides. The *n*- and *p*-contacts are annealed for 80 s at 380 °C and 350 °C, respectively. A 1-µm-thick SiN_x dielectric layer is deposited by PECVD on the whole wafer for electrical isolation. This layer is then opened before the Ti/Au probe pads deposition. A typical cross-sectional SEM (Scanning Electron Micrograph) image of hybrid structures and an optical microscope image of the device after completed fabrication are shown in Fig. 5(a) and Fig. 5(b), respectively.

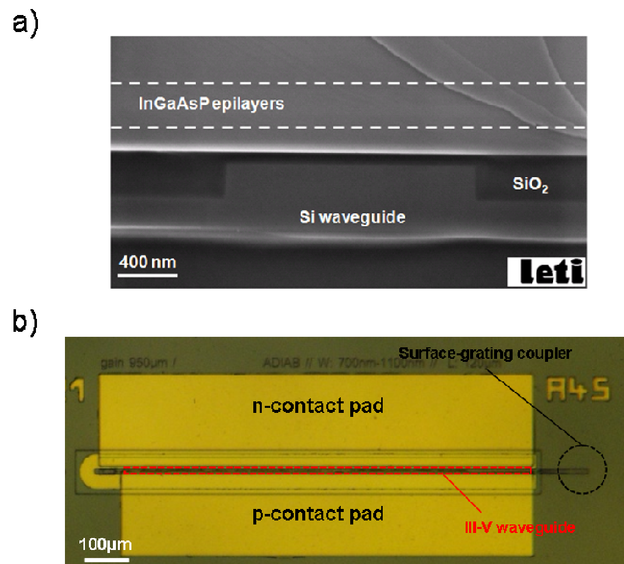

Fig. 5. a) Cross-sectional SEM image of a hybrid structure before metallization. b) Top-view optical microscope image of a Si/III-V laser at the end of fabrication process.

3. Experimental results and discussion

The wafer is mounted on a thermoelectric cooler with a nominal set temperature adjusted to 20 °C. The hybrid laser is electrically pulse-pumped by applying a positive bias voltage to the upper electrical *p*-contact. The width and the period of the injected electrical current are 100 ns and 1 µs, respectively. The laser beam output is collected through the surface grating coupler by a multimode fiber and then characterized by using both a spectrum analyzer and an optical power-meter. At the same time, the laser structure behavior is imaged with an infrared camera.

Infrared images of the hybrid Si/III-V laser, taken slightly below threshold and well above threshold, are presented in Fig. 6(a). Figure 6(b) shows the measured laser peak power intensity as a function of injected current. As can be seen from the *L-I* characteristic, the laser threshold is 100 mA, corresponding to a threshold current density J_{th} of 1.76 kA/cm^2 with a maximum output power of 7.2 mW at 435 mA. Considering the measured 3 dB coupling losses from the surface grating coupler and 2 dB in the fibered optical setup, we calculate a differential quantum efficiency of 11.8% at a stage temperature of 20 °C. Laser operation is obtained for duty cycles as high as 60%, i.e. by increasing the pulse width until 600 ns while maintaining the period fixed to 1 µs.

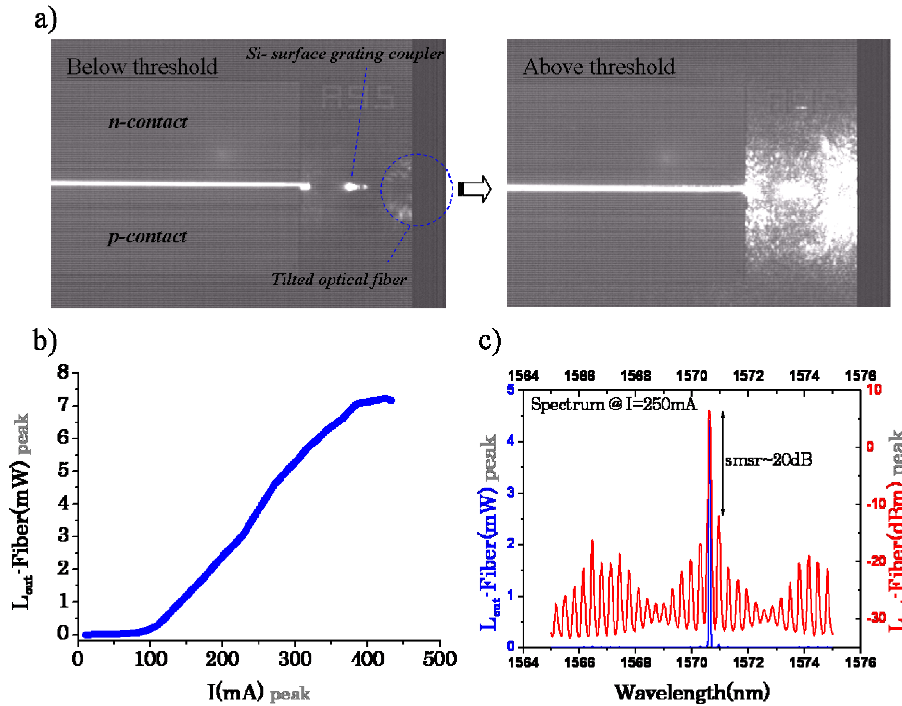

Fig. 6. a) Infrared images of the hybrid Si/III-V laser taken slightly below threshold (75 mA) and well above threshold (300 mA). b) Fiber coupled laser output as a function of drive current (*L–I* curve) of a 950-µm-long laser under pulsed operation, at 20 °C. The width and the period are 100 ns and 1 µs, respectively. c) Laser spectrum, linear and dB scales.

Figure 6(c) shows the measured multi-mode lasing spectrum at a drive current of 250 mA. The spectrum exhibits a Fabry-Pérot response with a free spectral range of 0.32 nm consistent with a modal group index of 3.62. The slowly varying envelope of the spectrum is attributed to back-reflections that occur at the entrance of the fiber. The lasing wavelength is around 1570 nm with a side-mode suppression ratio as high as 20 dB.

The evolution of the threshold current (in the pulsed regime) as a function of stage temperature yields a value for the characteristic temperature T_0 of 27K. Derivative analysis of the electrical characteristics gives a value of ~35 Ω for the series resistance. These data show that laser performances are currently limited by the unwanted heat generation caused by the high electrical series resistance. With particular attention spent on the contact metallurgy, this resistance value could likely be decreased by an order of magnitude [29]. Additionally, a major improvement in lasing threshold and differential efficiency could be made by using proton implant isolation for an efficient funnelling of carriers in the III-V heterostructure. The proton implant distribution could be enhanced to maximize the interaction strength between the optical mode and the injected carriers as well as to reduce the non-radiative surface recombinations that mostly occur on the sidewalls of the active waveguide. Considering the fabrication issues stated above, we expect that the CW regime could be attained with a lower threshold and a higher differential efficiency.

4. Conclusion

In this paper, we demonstrate the first hybrid silicon/III–V laser based on adiabatic mode transformers. The hybrid Fabry-Pérot laser cavity is designed to maximize the overlap between the III-V gain region and the optical supermode while maintaining a high coupling efficiency to the bottom Si waveguide, within the fabrication process tolerances.

The investigated device operates under quasi-continuous wave regime at room temperature with a threshold current of 100 mA, a side mode suppression ratio as high as 20 dB, a differential quantum efficiency of 11.8% and a fiber-coupled output power of ~7 mW.

For the time being, laser performances are limited by the series resistance of the electrical contacts and the lack of current confinement in the III-V waveguide. With more attention spent on the contact metallurgy and by incorporating a proton-implanted current aperture, we expect to obtain CW operation along with the improvement of laser performances in terms of current threshold and output power efficiency.

Acknowledgments

This work was supported by the French National “Nano 2012” project and sponsored by the EC-funded FP7-project HELIOS.